Scaling laws for the reduction of threading dislocation densities in homogeneous buffer layers

J. S. Speck,[a] M. A. Brewer, and G. Beltz[b]
Materials Department, University of California, Santa Barbara, California 93106

A. E. Romanov[c] and W. Pompe
Max Planck Gesellschaft, Arbeitsgruppe Mechanik Heterogener Festkörper, 01069 Dresden, Hallwachsstrasse 3, Germany

(Received 19 January 1996; accepted for publication 28 June 1996)

In the heteroepitaxial growth of films with large misfit with the underlying substrate (linear mismatch strains in excess of 1%–2%) the generation of misfit dislocations and threading dislocations (TDs) is ubiquitous for thicknesses well in excess of the equilibrium critical thickness. Experimental data suggest that the TD density in relaxed homogeneous buffer layers can be divided into three regimes: (i) an entanglement region near the film/substrate interface corresponding to TD densities of $\sim 10^{10}$–10^{12} cm^{-2}; (ii) a falloff in TD density that is inversely proportional to the film thickness h, applicable to densities in the range $\sim 10^{7}$–10^{9} cm^{-2}; and (iii) saturation or weak decay of the TD density with further increase in film thickness. Typical saturation densities are on the order of $\sim 10^{6}$–10^{7} cm^{-2}. In this article, we show that the TD reduction may be described in terms of effective lateral motion of TDs with increasing film thickness. An analytic model is developed that successfully predicts both the $1/h$ scaling behavior and the saturation of TD densities. Long-range fluctuations in the net Burgers vector content of the local TDs is a cause for saturation behavior. These models are supported by computer simulations. © *1996 American Institute of Physics.* [S0021-8979(96)04919-5]

I. INTRODUCTION

During the past 20 to 30 years, there has been a substantial effort to epitaxially grow a broad range of materials combinations. In semiconductor heteroepitaxy, the choice of a substrate is dictated by its availability in single crystals, its suitability for the application (e.g., with regard to processing, band gap, and chemical compatibility), and its cost. While the substrate constraints offer some flexibility, the choice of material for the film is generally dictated by the application itself and hence determines the crystal structure and lattice parameter of the film. In many cases the active device layer may have a substantial lattice misfit with the substrate which means that there is a possibility of formation of misfit dislocations (MDs) at the film/substrate interface. Threading dislocations (TDs) accompany the formation of MDs and often find their way into the active region of electronic and optoelectronic devices. Generally, TDs degrade the physical properties of devices. Thus it is of great importance to establish effective means for the elimination or reduction of TD densities.

In this article, we will develop geometrically motivated scaling laws for TD density reduction in homogeneous buffer layers. This framework has its foundation in the assumption that TD densities are primarily reduced by reactions between pairs of TDs that either lead to annihilation or result in one TD (fusion reactions). The model assumes three regimes: entanglement; $1/h$ scaling; and saturation. The entanglement region corresponds to the highest dislocation densities near the film/substrate interface where physical models for annihilation are difficult to apply or study experimentally. The $1/h$ region has a geometric basis in that dislocation annihilation requires different minimum energy growth trajectories for the TDs with the same Burgers vector thus giving rise to effective relative lateral motion of the TDs with increasing film thickness. The saturation behavior is attributed to local fluctuations in TD densities—possibly as a result of early MD generation processes. The simple scaling laws for TD reduction that we develop are consistent with several experimental reports.

II. BACKGROUND

Although there remain many open questions on dislocation generation in epitaxial growth, we will only consider the behavior of TDs that are formed as a consequence of the film growth and MD generation. Regardless of the growth mode for mismatched films (i.e., Frank–van der Merwe (layer-by-layer), Stranski–Krastanow (initial wetting followed by islanding), or Volmer–Weber (incoherent islanding) growth) increasing film thickness will ultimately lead to MD generation and concomitant TDs. The mismatched film will grow strained but dislocation-free until it reaches a kinetic critical thickness h_k in excess of the equilibrium critical thickness h_c, whence dislocations nucleate to relieve the strain. The concepts of equilibrium critical strained layer thicknesses were first introduced by Frank and van der Merwe and then developed by Matthews and Blakeslee in a dislocation framework and have been extended by several other investigators (see, for example, the recent work of Freund[1]). For a fully relaxed film, the linear MD density $\rho_{\mathrm{MD,relaxed}}$ multi-

[a]Electronic mail: speck@surface.ucsb.edu
[b]Mechanical Engineering Department.
[c]Permanent address: A.F. Ioffe Physico-Technical Institute, Russian Academy of Sciences, 194021 St. Petersburg, Russia.

 0021-8979/96/80(7)/3808/9/$10.00

plied by the edge component of the MD Burgers vector parallel to the interface $b_{\text{edge},\parallel}$ is equal to the misfit strain ϵ_m:

$$\rho_{\text{MD,relaxed}} b_{\text{edge},\parallel} = \epsilon_m . \tag{1}$$

For films of finite thickness that are grown on semi-infinite substrates, the equilibrium linear MD density $\rho_{\text{MD,equil}}$ may be readily shown to scale in the following manner:[2]

$$\rho_{\text{MD,equil}} = \rho_{\text{MD,relaxed}} \left(1 - \frac{h_c}{h} \right). \tag{2}$$

In the heteroepitaxial growth of semiconductors with large lattice mismatches, e.g., $\epsilon_m > \sim 2\%$, the critical thicknesses are on the order of 25 Å and dislocation generation is ubiquitous for layer thicknesses much in excess of h_c (i.e., MDs an associated TDs are generated when $h = h_k$). For the modeling of TD reduction, we assume cases in which $h \gg h_k > h_c$ and thus further strain relaxation within a homogeneous layer by the long-range glide of the threading segments will be neglected.

For layer-by-layer growth, the prevailing assumption is that dislocation half-loops nucleate at steps or impurities on the growing free surface,[3–5] and the loops expand to form two threading segments, largely of screw character, with antiparallel Burgers vectors, and a misfit segment at the film/substrate interface. Thus, the initial TD density is twice the nuclei density. For TD segments in epitaxial layers, we adopt the convention that the dislocation line direction is in the same sense as the film/substrate surface normal. This convention is used because in large mismatch heteroepitaxy it is practically impossible to identify matching pairs of threading dislocations from the same nucleation event, that is, isolated loops are rarely, if ever, discernible. We note here that for $h > h_c$, the MDs are equilibrium interfacial defects with an equilibrium population given approximately by Eq. (2). On the contrary, the TDs in all cases raise the free energy of the film—the equilibrium density of these defects is zero.

In typical large mismatch semiconductor heteroepitaxy, the TD density is very high near the film/substrate interface and decreases with increasing film thickness. An example of epitaxial GaAs on Si(001) is shown in the lower region of Fig. 1. The TD density is $\sim 10^{10}$ cm^{-2} near the film/substrate interface and begins to fall throughout the GaAs buffer. For the CdZnTe layer on ZnTe in Fig. 1, again, the TD density is almost immeasurably high near the CdZnTe/ZnTe interface, then it begins to fall with increasing film thickness. In fact, it is frequently difficult to distinguish micrographs from different lattice mismatched materials provided that the materials have the same growth orientation and slip systems. Thus, this motivates a geometrically-based model for TD reduction.

In recent years there have been several efforts to quantify the thickness dependence of the TD density for lattice mismatched growth. Sheldon *et al.* reported on the thickness dependence of the TD density for the systems InAs/GaAs, GaAs/Ge/Si, GaAs/InP, and InAs/InP.[6] These systems represented a range of lattice and thermal expansion mismatches between the film and the substrate. It was found that the TD density was proportional to the inverse of the film thickness for TD densities on the order of $\sim 10^8$–10^9 cm^{-2}. Further, the thickness dependence of the densities were found to all fall on the same curve, independent of specific epilayer/substrate combination, as shown in Fig. 2(a). In a similar study, Tachikawa and Yamaguchi also observed $1/h$ (where h is the film thickness) behavior for the TD density in thick films of GaAs-on-Si.[7] However, at lower dislocation densities, a weaker decay was observed, as shown in Fig. 2(b). Further, in the study of strained layer superlattices, TD densities have commonly been observed to saturate for larger film thickness.[8–10] We do not intend to review the wealth of experimental data on threading dislocations and approaches to their reduction in lattice mismatched epitaxy. Rather, the goal of this paper is to develop a physically-based model to explain the $1/h$ behavior for TD density and to discuss possible origins for the saturation or exponential decay behavior for large film thicknesses.

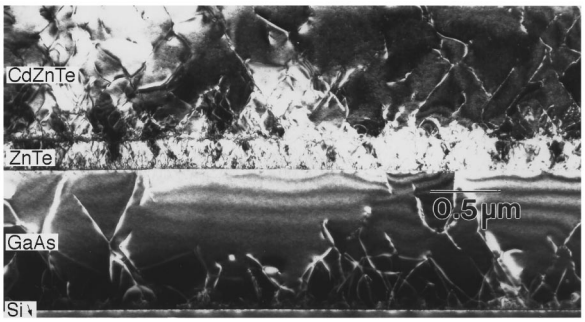

FIG. 1. Cross-section transmission electron micrographs showing typical threading dislocation structures and rapid falloff with increasing layer thickness in each layer for $Cd_{1-x}Zn_xTe$ (top layer)/ZnTe (/GaAs/Si(001). This strong two-beam dark bright-field images was recorded near a [110] zone axis with $\mathbf{g}=004$.

III. CONCEPT OF DISLOCATION REDUCTION

The geometrical requirement that dislocation lines may end only at free surfaces, high-angle grain boundaries, or other dislocations is a restriction that must be obeyed in all models for dislocation reduction. For example, we can immediately exclude the physically incorrect possibility that TDs may end abruptly in a film without joining with another defect. Further, we treat the problem of threading reduction assuming a semi-infinite substrate, and thus we intentionally neglect the possibility of TDs leaving the edges of the thin film. Thus we work in the limit that TD densities are reduced by either annihilation of threading segments with antiparallel Burgers vectors or by reactions in which two TDs combine to form one TD (referred to hereon as fusion reactions). For example, annihilation would result from the reaction of two TDs with Burgers vectors $a/2[101]$ and $a/2[\bar{1}0\bar{1}]$. An example of fusion would be the energetically favorable reaction between two TDs with Burgers vectors $a/2[101]$ and $a/2[011]$ leading to a single new threading segment with Burgers vectors $a/2[110]$.

We work with the further assumption that the TDs maintain glissile orientations, i.e., after nucleation TDs stay on

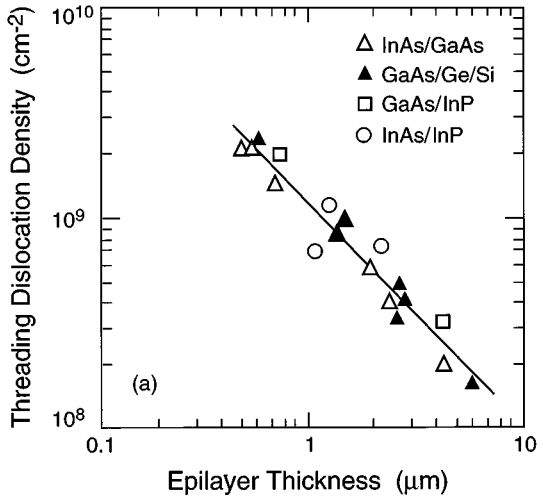

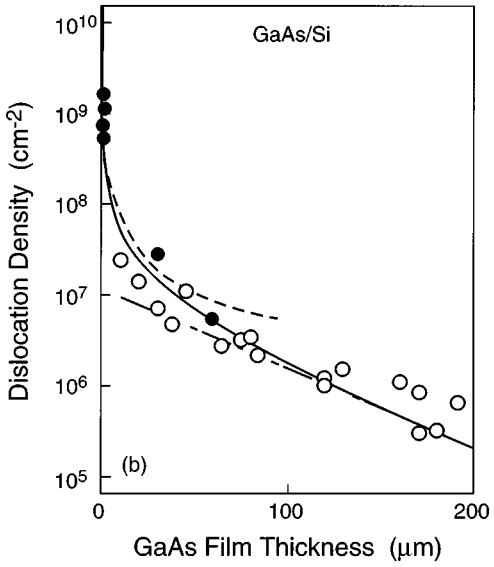

FIG. 2. Experimental data, reported in the literature, showing the scaling of the threading dislocation density with increasing film thickness. (a) Results of a study showing the universal $1/h$ decay of the TD density for high dislocation densities for a range of systems [after Sheldon *et al.* (see Ref. 6)]. (b) Results of a study showing both the $1/h$ decay of the TD density for high dislocation densities and either saturation or exponential decay behavior of the TD density of thick films [after Tachikawa and Yamaguchi (see Ref. 7)].

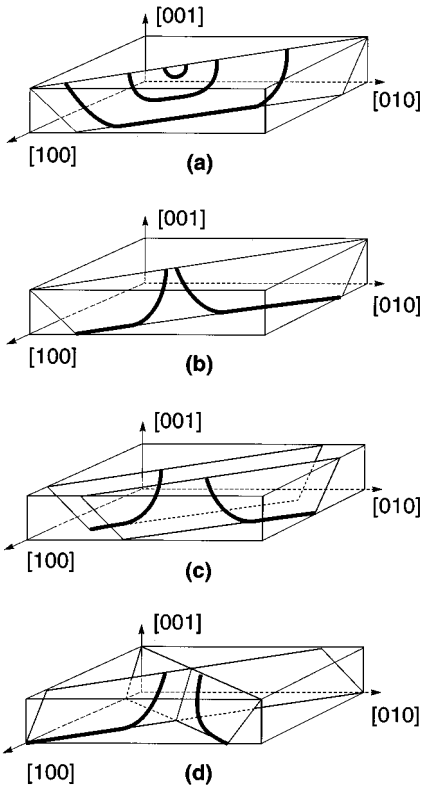

FIG. 3. Possible processes for annihilation of threading dislocations in a dislocated epitaxial film. (a) Loops can self-annihilate. (b) Threading segments from different dislocation sources on the same slip plane can annihilate. (c) Threading segments from different dislocation sources on the parallel slip systems can annihilate. This may be accomplished by conservative dislocation motion, namely glide and cross slip. Alternatively, annihilation may be achieved entirely by glide and climb of the threading segments. (d) Threading segments from different dislocation sources on intersecting slip systems can annihilate by glide or by climb or a combination of both glide and climb.

their natural slip plane. The annihilation or fusion reactions may happen in the following ways (shown schematically in Fig. 3):

(a) Loops can self-annihilate by glide.
(b) Threading segments from different dislocation sources on the same slip plane can either annihilate or fuse by glide.
(c) Threading segments from different dislocation sources on the parallel slip systems can either annihilate or fuse. This may be accomplished by conservative dislocation motion, namely, glide and cross slip. Alternatively, TD reduction reactions may be achieved entirely by glide and climb of the threading segments.
(d) Threading segments from different dislocation sources on intersecting slip systems can annihilate or fuse by glide or climb or a combination of glide and climb.

The process of annihilation may now be considered sequentially. In Fig. 3(a), a pair of TDs and the associated MD are shown. The antiparallel threading segments and the MD form one continuous dislocation line. In principle, if the misfit strain in the film changes (for example, through differential thermal expansion or by diffusion), then the threading segments may close back on one another to form a closed loop (also shown). However, in the absence of any strain reversal, loop self-closure leads to no far field strain relief. Thus, this process of threading annihilation is considered unviable. In Fig. 3(b), the geometry is shown for threading segments generated from separate sources on the same specific slip plane. In this case, the two threading segments have an opposite sense and will annihilate upon contact. It is this process of annihilation or fusion of TDs nucleated from separate sources that ultimately leads to dislocation reduction. However, the likelihood of having independent nucleation events on precisely the same slip plane is considered to be vanishingly small, and thus this mechanism is unlikely despite its obvious illustrative appeal.

Annihilation or fusion of threading segments generated

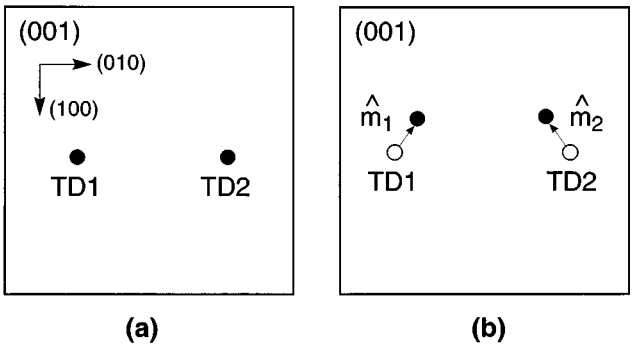

FIG. 4. Effective motion of TDs in the (001) epitaxy of cubic semiconductors. The intersection point of the TDs with the free surface changes with increasing film thickness. TD1 has a Burgers vector $a/2[101]$ and lies on the $(1\bar{1}1)$ plane with a $[112]$ line direction, TD2 has a Burgers vector $a/2[101]$ and lies on the (111) plane with a $[\bar{1}\bar{1}2]$ line direction. (a) Position of TD1 and TD2 at film thickness h_1 and (b) position of TD1 and TD2 at film thickness h_2. The vectors $\mathbf{m_1}$ and $\mathbf{m_2}$ are unit vectors in the plane of the film surface and represent the direction of motion of the TDs on the film surface with increasing film thickness.

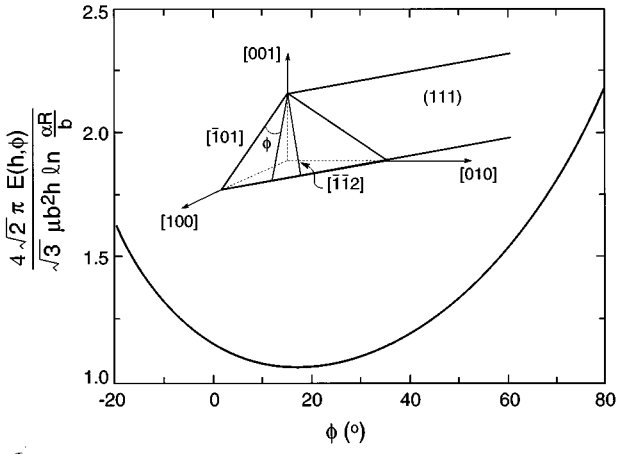

FIG. 5. Orientational dependence for the total energy of a threading dislocation with Burgers vector $a/2[101]$ in a film of thickness h. The film normal is [001] and (111) is the specific slip plane. Isotropic elasticity was used for these calculations with $\nu=0.3$. The inset perspective drawing shows the orientation of a TD with $\mathbf{b}=a/2[101]$ on a (111) plane in an (001) epitaxial film.

from separate sources, but within some close proximity, appears to be most probable physical process for dislocation reduction. There are two simple possibilities for this case: the threading segments lie on parallel slip planes, as shown in Fig. 3(c), or they lie on intersecting slip planes as shown in Fig. 3(d). Threading segments on parallel slip planes can annihilate or fuse by conservative motion in which one of the threading segments assumes a pure screw orientation, cross slips onto the slip plane of the other threading segment, and then glides to the other threading segment. Alternatively, the threading segments can move to a minimum separation distance by glide and then climb together. For the case of threading segments on intersecting slip planes, annihilation or fusion can be achieved by glide alone. We argue below that this is the most likely and efficient mechanism for annihilation, but first some specific geometrical considerations are necessary.

The $a/2\langle 110\rangle\{111\}$ slip system is the most important and common for dislocations in either diamond or zinc-blende semiconductors. If the TDs are glissile, then for [001] growth they will lie on one of four {111} slip planes. With evolving film growth, the TDs are inclined and their intersection point with the free surface moves with increasing film thickness, as shown schematically in Fig. 4. Thus, without glide, there is effective lateral motion of the TDs with increasing film thickness.

The minimum energy configuration of a straight TD is a balance between maximizing its screw nature while concurrently minimizing the total line length. For a film of thickness h, consider the minimum energy orientation of a threading segment with $\mathbf{b}=a/2[101]$ lying on a (111) glide plane. The line length of a pure screw segment in this case is given as $\sqrt{2}\cdot h$. Using the pure screw orientation as the reference orientation, the energy of an arbitrarily oriented threading segment may be calculated in the line tension approximation[11] and is given as

$$E(h,\phi)=\frac{\mu b^2}{4\pi}\frac{\sqrt{3}h}{\sqrt{2}\,\cos(\pi/6-\phi)}\times\left(\cos^2\phi+\frac{\sin^2\phi}{1-\nu}\right)\ln\left(\frac{\alpha R}{b}\right), \tag{3}$$

where ϕ is the angle between the threading segment and the $[101]$ direction, μ is the shear modulus, and R is a length that is determined by the mean spacing between TDs but also weakly depends on h and ϕ. Since R is in the argument of the logarithm, we neglect any R dependence on $E(h,\phi)$. We note that the minimum TD line length corresponds to a $[112]$ line direction. A plot of this energy for $\nu=0.3$ is shown in Fig. 5. It can be seen that the minimum energy orientation is $\sim 15°$ away from the screw orientation in the direction that reduces its line length.

Now we consider the geometry of the full set of possible glissile threading dislocations for the (001) epitaxy of cubic semiconductors. Again, the slip system in the film will be given as $a/2\langle 110\rangle\{111\}$. Thus, there are four unique {111} planes and six unique $\langle 110\rangle$ directions. Considering that the dislocation Burgers vectors can assume either positive or negative sense, there are 12 possible Burgers vectors. Finally, a glissile dislocation with an $a/2\langle 110\rangle$ Burgers vector can have its line in one of two possible {111} planes and thus there are a total of 24 specific dislocation Burgers vector/slip plane combinations. In Fig. 6 the geometry of the TDs is shown both in perspective and in projection along [001]. The position of the intersection of specific TDs with the free surface of the film is denoted with a symbol shown in the figure. Additionally, a reaction table between all of the possible Burgers vectors for the TDs is given in Table I. Details of this table will be discussed shortly.

The inclined orientation of the TDs leads to a geometrically governed situation in which the threading segments that lie on intersecting slip planes will have a minimum separation distance with increasing film thickness. Consider again

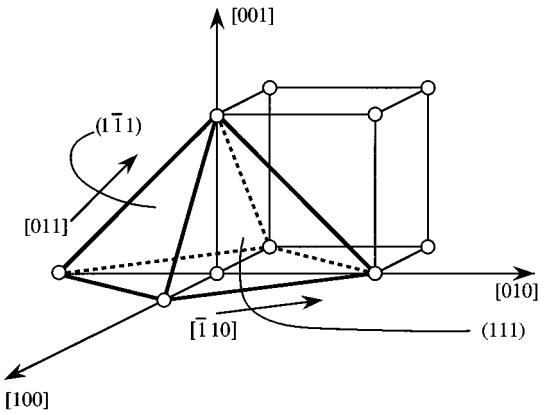

FIG. 6. Slip geometry for $a/2\langle 110\rangle\{111\}$ systems for (001) epitaxial films. The four inclined {111} planes and the inclined $a/2\langle 101\rangle$ edges of the half-octahedron represent the active slip systems for surface nucleation of MDs and TDs.

the specific example shown in Fig. 4. TD1 lies on the $(1\bar{1}1)$ plane and has a Burgers vector $a/2[101]$, TD2 lies on the (111) plane and has Burgers vector $a/2[101]$. At film thickness h_1, TD1 and TD2 are separated by a distance r_1, at film height h_2 the TDs are separated by a distance r_2. If the TDs come within a distance such that the interaction force is sufficient to initiate thermally assisted glide, then the dislocations will begin to move together and subsequently annihilate or fuse. The minimum distance necessary to initiate glide depends on the kind of possible reaction between defects and is referred to as the annihilation radius r_A or the fusion radius r_F. The concept of an annihilation radius has been developed earlier by Kusov and Vladimirov[12] and by Martisov and Romanov[13] and used by the latter researchers in TD reduction problems.

A simple estimation of the annihilation radius can be obtained by comparing the elastic force acting between two dislocations with the friction force caused by the Peierls stress σ_p. Balancing these forces gives $r_A \approx \mu b/2\pi\sigma_p$. For usual values of $\sigma_p \approx 10^{-3}-10^{-4}\ \mu$, $r_A \approx 10^2-10^3\ b$, or $r_A \approx 500-5000$ Å. The inclined orientation of the threading segments leads to effective lateral motion of the TDs, in this case with increasing film thickness. Virtually all successful approaches to reducing TD density rely on enhancing the effective lateral motion of TDs such that the TDs will fall within an annihilation or fusion radius of one another. This is the essential concept of TD reduction.

To find the value of the r_A or r_F we must solve the complicated problem of the interaction of two angular TD-MDs near a free surface. Factors such as temperature, Peierls barrier, internal and externally imposed stresses, presence of point defects must all be considered. For the current investigation, we will treat r_A and r_F as constant parameters. Film thickness and dislocation densities are then normalized to r_A and r_A^{-2}, respectively. Before a reaction commences, a TD has no degrees of freedom (its motion is determined by the minimum line energy orientation). After the reaction begins, TDs may either cross slip or climb, thus providing the TDs with additional degrees of freedom.

IV. POSSIBLE REACTIONS BETWEEN THREADING DISLOCATIONS IN CUBIC SEMICONDUCTORS

Before the scaling laws are developed, it is instructive to consider possible reactions between undissociated glissile threading dislocations. Since the energy per unit length of a dislocation is proportional to b^2, we will use this as an initial criteria in the reactions. In Table I, reactions between the 12 possible TD Burgers vectors are shown for the slip system $a/2\langle 101\rangle(111)$ applicable to the (001) growth of a cubic semiconductor. The first eight Burgers vectors (in either the columns or rows) may result from surface nucleation of half-loops. The final four Burgers vectors combinations in Table I have Burgers vectors that are parallel to the film/substrate interface and result from fusion reactions between TDs with inclined Burgers vectors. The entries in Table I with a **0** correspond to annihilation; entries denoted with an **X** correspond to unfavorable reactions and also repulsive interactions; entries with a specific resultant Burgers vector correspond to fusion reactions; finally, entries designated **N**

TABLE I. Possible reactions between threading dislocations in the epitaxy of cubic semiconductors. The TDs have $a/2\langle 101\rangle$ type Burgers vectors. Table entries for complete annihilation reactions are indicated by **0**, the resulting dislocation Burgers vector is shown for half-annihilation reactions, repulsive interactions are shown with an **X**, energetically unfavorable reactions are shown by **N**. TDs 1 through 8 correspond to those generated by surface half-loop nucleation. TDs 9 through 12 correspond to those generated either by island growth or fusion reactions.

	$\mathbf{b}_1\backslash\mathbf{b}_2$	1 $a/2[101]$	2 $a/2[10\bar{1}]$	3 $a/2[\bar{1}01]$	4 $a/2[\bar{1}0\bar{1}]$	5 $a/2[011]$	6 $a/2[0\bar{1}1]$	7 $a/2[01\bar{1}]$	8 $a/2[0\bar{1}\bar{1}]$	9 $a/2[110]$	10 $a/2[\bar{1}10]$	11 $a/2[1\bar{1}0]$	12 $a/2[\bar{1}\bar{1}0]$
1	$a/2[10\bar{1}]$	**X**	**0**	**N**	**N**	**X**	$a/2[\bar{1}10]$	**X**	$a/2[110]$	**X**	$a/2[0\bar{1}1]$	**X**	$a/2[011]$
2	$a/2[\bar{1}01]$	**0**	**X**	**N**	**N**	$a/2[\bar{1}10]$	**X**	$a/2[\bar{1}10]$	**X**	$a/2[011]$	**X**	$a/2[0\bar{1}1]$	**X**
3	$a/2[10\bar{1}]$	**N**	**N**	**X**	**0**	**X**	$a/2[\bar{1}10]$	**X**	$a/2[\bar{1}10]$	$a/2[011]$	**X**	$a/2[011]$	**X**
4	$a/2[\bar{1}01]$	**N**	**N**	**0**	**X**	$a/2[\bar{1}10]$	**X**	$a/2[\bar{1}10]$	**X**	**X**	$a/2[0\bar{1}1]$	**X**	$a/2[011]$
5	$a/2[011]$	**X**	$a/2[\bar{1}10]$	**X**	$a/2[\bar{1}10]$	**X**	**0**	**N**	**N**	**X**	$a/2[\bar{1}01]$	$a/2[\bar{1}01]$	**X**
6	$a/2[0\bar{1}1]$	$a/2[\bar{1}10]$	**X**	$a/2[\bar{1}10]$	**X**	**0**	**X**	**N**	**N**	$a/2[\bar{1}01]$	**X**	**X**	$a/2[\bar{1}01]$
7	$a/2[01\bar{1}]$	**X**	$a/2[\bar{1}10]$	**X**	$a/2[\bar{1}10]$	**N**	**N**	**X**	**0**	$a/2[\bar{1}01]$	**X**	**X**	$a/2[\bar{1}01]$
8	$a/2[011]$	$a/2[\bar{1}10]$	**X**	$a/2[\bar{1}10]$	**X**	**N**	**N**	**0**	**X**	**X**	$a/2[\bar{1}01]$	$a/2[\bar{1}01]$	**X**
9	$a/2[\bar{1}10]$	**X**	$a/2[01\bar{1}]$	$a/2[01\bar{1}]$	**X**	**X**	$a/2[\bar{1}01]$	$a/2[\bar{1}01]$	**X**	**X**	**0**	**N**	**N**
10	$a/2[\bar{1}\bar{1}0]$	$a/2[01\bar{1}]$	**X**	**X**	$a/2[0\bar{1}\bar{1}]$	$a/2[\bar{1}01]$	**X**	**X**	$a/2[\bar{1}01]$	**0**	**X**	**N**	**N**
11	$a/2[1\bar{1}0]$	**X**	$a/2[0\bar{1}\bar{1}]$	$a/2[011]$	**X**	$a/2[\bar{1}01]$	**X**	**X**	$a/2[\bar{1}01]$	**N**	**N**	**X**	**0**
12	$a/2[\bar{1}\bar{1}0]$	$a/2[011]$	**X**	**X**	$a/2[01\bar{1}]$	**X**	$a/2[\bar{1}01]$	$a/2[\bar{1}01]$	**X**	**N**	**N**	**0**	**X**

correspond to possible reactions between two TDs with perpendicular Burgers vectors, the b^2 criteria is not applicable for these reactions; rather, the possible reactions may be governed by a balance between core energy and line length minimization. A complete treatment of the problem also includes the specific slip planes for the TDs and this leads to a total of 24 specific TD/slip plane combinations. Such a treatment will be presented in a separate paper.

Table I is a useful tool for discussing the physical processes of TD reduction. The upper left 8×8 entries correspond to reactions between primarily generated TDs, i.e., the sets of reactions between TDs initially generated from surface nucleation. From the entries, it is easy to see that of the eight reactions one leads to annihilation, two to fusion, and five are unfavorable and may lead to changes in the slip plane of the TDs by cross slip. The two fusion reactions, e.g., $a/2[101]+a/2[011]\rightarrow a/2[110]$, between primary TDs lead to TDs with Burgers vectors parallel to the film/substrate interface. These secondary TDs can react with the primary TDs, in this case leading to either repulsion for one half of the reactions or further fusion reactions for the other half of the reactions; these entries are given in the 8×4 entries in the upper right hand corner of the table and the 4×8 entries in the lower left hand corner of the table. Finally, reactions between the secondary TDs, given in the lower 4×4 entries in the table, can lead to either annihilation (one fourth of the entries), one fourth lead to repulsion, and since the secondary TDs may have perpendicular Burgers vectors, one half of the possible reactions correspond to no reaction.

V. DEVELOPMENT OF SCALING LAWS FOR THREADING DISLOCATION REDUCTION

The entanglement region corresponds to the film nearest to the substrate where the TD density is often on the order of 10^{10}–10^{12} cm^{-2} (e.g., see Fig. 1). At such high densities, individual TDs are difficult to resolve, even by weak beam TEM imaging techniques. When individual TDs are resolvable by TEM, it is difficult to determine their geometry in the foil and their reactions with other TDs. In close analogy to highly cold worked metals, where dislocation forests can form, we call this the entanglement region. With increasing film thickness, the dislocation density falls off quickly, in a manner that has yet to be determined and the mean TD spacing becomes larger than either the annihilation or fusion radius. We believe that modeling the TD reduction in this region represents the area with the least possibility of successfully describing the physical behavior.

We begin by assuming that the threading dislocations have minimum energy orientations that allow annihilation or fusion reactions with changing film thickness. With increasing film thickness, the separation distance between the TDs will change, and at some film thickness, a minimum separation distance will be achieved between TDs with different Burgers vectors. If the approach distance between two TDs with different Burgers reaches a value in which the TDs begin to glide together because of the attractive force field, the TD will come together and annihilate or fuse, this separation distance is given as the annihilation radius r_A or the fusion radius r_F.

The governing differential equation for TD reduction may be derived, for simplicity, by considering only annihilation reactions. In projection, each TD will sweep out an interaction area $S=2r_A \tan\psi\Delta h$ with change in thickness Δh, where ψ is the angle between the TD line direction and the surface normal. Each TD will encounter $N=\rho S$ other TDs and thus $\Delta\rho=-N\rho=-\rho^2 S=-2r_A \tan\psi\ \rho^2\Delta h$. Taking the limit that Δh becomes vanishingly small leads to the differential equation:

$$d\rho=-2r_A \tan\psi\rho^2 dh. \tag{4}$$

A further geometrical consideration leads to a final modification to the coefficient in Eq. (4). The TDs that will interact must have net relative motion, which can be characterized by a factor $M=|\tan\psi_i\mathbf{m}_i-\tan\psi_j\mathbf{m}_j|$, where $\mathbf{m}$ is a unit vector that gives the lateral motion of TDs i and j on the film surface with changing film thickness, see Fig. 4. With this modification, we can write the overall equation for TD reduction as

$$d\rho=-K\rho^2 dh, \tag{5}$$

where $K=2r_A\overline{M}$ and $\overline{M}$ represents the average value of the net relative of motion of all possible pairs of TDs with changing film thickness. Equation (5) may be integrated as follows:

$$\int_{\rho_0}^{\rho}\frac{1}{\rho^2}\,d\rho=-K\int_{h_0}^{h}dh, \tag{6}$$

where ρ_0 is the threading dislocation density at h_0 and h_0 is the starting thickness and usually can be taken as the thickness for which the average spacing between threading dislocations is larger than the annihilation radius r_A. This directly leads to

$$\rho=\frac{1}{K(h-h_0)+1/\rho_0}. \tag{7}$$

With the definition: $\hat{h}\equiv 1/K\rho_0-h_0$, Eq. (7) simplifies to

$$\rho=\frac{1/K}{h+\hat{h}}. \tag{8}$$

When $h\gg\hat{h}$, the threading dislocation density is inversely proportional to the film thickness, i.e.,

$$\rho=\frac{1}{Kh}. \tag{9}$$

This simple approach thus predicts the $1/h$ scaling behavior. If we set K equal to twice the annihilation radius $2r_A$ ($M=1$), we may readily solve for $\hat{h}$. For instance, if the initial threading dislocation density is 10^{10} cm^{-2}, $h_0=0$ (for simplicity) and the annihilation radius is 500 Å, then $\hat{h}$ has a value of 1000 Å. If we assume $h\gg\hat{h}$, Eq. (9) would be valid for thicknesses on the order of 1 μm and larger, this is in close agreement with the initial thicknesses for which TD densities are commonly reported. We note that the Sheldon *et al.* data shown in Fig. 2(a) correspond to an r_A value of ~500 Å and the Tachikawa and Yamaguchi data shown in Fig. 2(b) correspond to an r_A value of ~1000 Å. Note that these values of the annihilation radius are in reasonable

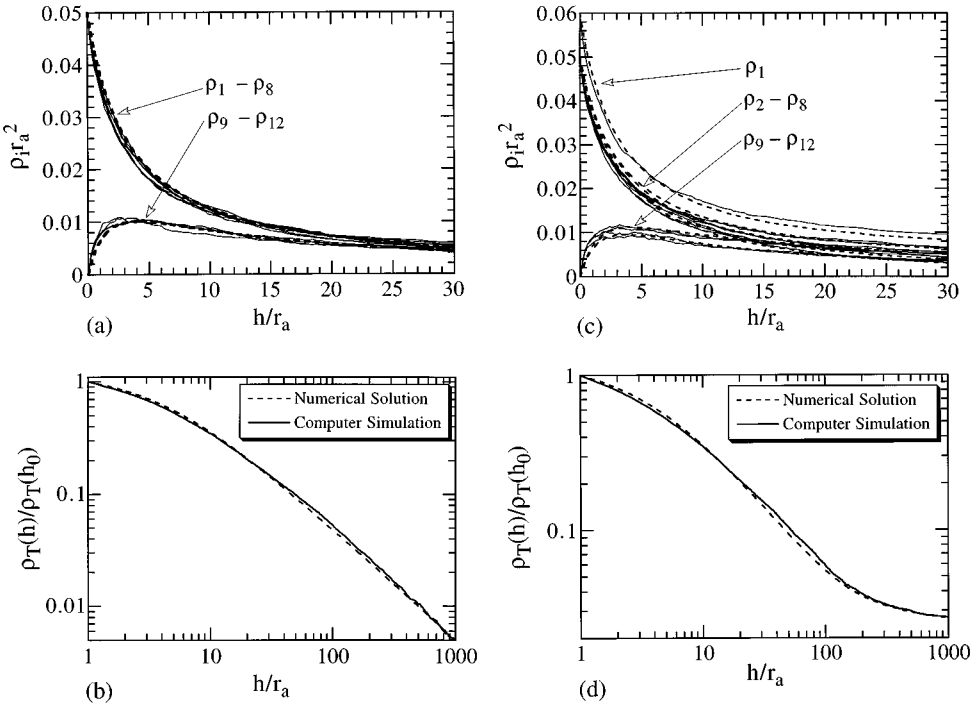

FIG. 7. Dependence of threading dislocation density on film thickness, numerical solutions (dashed lines) and results of computer simulation for (a,b) balanced initial TD density and for (c,d) unbalanced initial TD density. (a) and (c): Thickness dependence of TD density for each type of TD (linear scale). The densities are given in units of r_A^{-2}. (b) and (d): Total TD density, log-log scale. The normalized total density is shown, i.e., $\rho_T(h)/\Sigma_{j=1}^{12}\rho_j(h_i)$. The thickness in all of these plots is normalized by r_A. Initial dislocation densities: (a),(b): $\rho_1=\rho_2=\ldots=\rho_8=0.05/r_A^2$; $\rho_9=\rho_{10}=\rho_{11}=\rho_{12}=0$. (c),(d): $\rho_1=0.06/r_A^2$, $>\rho_2=\rho_3=\rho_4=\rho_5=\rho_6=\rho_7=\rho_8=0.05/r_A^2$, $\rho_9=\rho_{10}=\rho_{11}=\rho_{12}=0$. For the numerical solutions, the parameters were set such that $r_A=r_F$ and $M=1$. For the balanced case (b) note that the slope is -1 for thicknesses larger than $\sim 10r_A$. For the unbalanced case (d), note that the slope is approximately -1 for roughly one decade of thickness and then decreases for $h>200r_A$ and the density then saturates for increasing h.

agreement with the simple estimation based on the force balance between attractive force for two TDs and the friction force due to the Peierls stress σ_p (see above).

Table I can be used to write a system of 12 coupled, first-order, nonlinear, ordinary differential equations for the TD densities. If we consider the reactions that directly impact the density of TDs with Burgers vector $a/2[101]$ (designated 1 throughout Table I or simply as ''1'' here), then $1+2\rightarrow 0$ (annihilation); $1+2\rightarrow 11$ (fusion); $1+8\rightarrow 9$; $1+10\rightarrow 7$; and $1+12\rightarrow 5$. These reactions all reduce ρ_1. However, 1 may be generated by the following reactions: $5+11\rightarrow 1$ and $7+9\rightarrow 1$. Thus the first differential equation in this system of 12 equations may be written as

$$\frac{d\rho_1}{dh} = -K_{1,2}\rho_1\rho_2 - K_{1,6}\rho_1\rho_6 - K_{1,8}\rho_1\rho_8 - K_{1,10}\rho_1\rho_{10} - K_{1,12}\rho_1\rho_{12} + K_{5,11}\rho_5\rho_{11} + K_{7,9}\rho_7\rho_9, \tag{10}$$

where the $K_{m,n}$ coefficients correspond to the specific reaction cross sections. This equation can be simplified substantially by assuming that there are only two relevant cross sections: those for annihilation and those for fusion, thus eqn. 10 can be rewritten as

$$\frac{d\rho_1}{dh} = -2r_A\overline{M}\rho_1\rho_2 - 2r_F\overline{M}\rho_1(\rho_6+\rho_8+\rho_{10}+\rho_{12}) + 2r_F\overline{M}(\rho_5\rho_{11}+\rho_7\rho_9), \tag{11}$$

where $2r_A\overline{M}$ has replaced $K_{1,2}$ and $2r_F\overline{M}$ has replaced all coefficients for fusion reactions, r_F is the fusion radius, and the coefficient M accounts for geometrical factors of relative dislocation motion. Equation (11) is representative of one of the 12 equations in the system.

Numerical solutions for the system of coupled differential equations for TD density can readily be obtained using standard mathematical software. This capability facilitates an understanding of many of the general features of TD reduction. To illustrate solutions, first consider the case in which the initial TD density corresponds to equal populations of TDs with inclined Burgers vectors, i.e., TDs 1 through 8 in Table I, and zero initial population of TDs with Burgers vectors parallel to the film/substrate interface, i.e., $\rho_9(h_0)$ through $\rho_{12}(h_0)=0$. The thickness dependence of the individual TD densities is shown in a linear plot in Fig. 7(a) (dashed lines). Note that ρ_1 through ρ_8 all decrease monotonically with increasing film thickness. However, ρ_9 through ρ_{12} initially increase very rapidly, then also begin to fall with increasing h. The initial increase in ρ_9 through ρ_{12} is due to fusion reactions amongst TDs 1 through 8. The reduction in the total TD density, ρ_T, with increasing h can be seen in the log-log plot in Fig. 7(b). The slope of $\log\rho - \log h$ approaches -1 for large h. Thus, even when a more complete crystallographic treatment is taken into account, the total TD density follows the same behavior $(1/h)$ as predicted with the simplified model [Eq. (9)]. Note that no saturation behav-

ior is observed for this case; rather, ρ_T continues to decrease with increasing film thickness.

It is also instructive to consider cases in which the initial TD densities are unbalanced such that the film has a net Burgers vector content. Solutions to the system of coupled differential equations are shown in Figs. 7(c) and 7(d) for a case for which the initial TD densities at h_i are given as $\rho_1 > \rho_2 = \rho_3 = \rho_4 = \rho_5 = \rho_6 = \rho_7 = \rho_8 = \rho_i$ and $\rho_9 = \rho_{10} = \rho_{11} = \rho_{12} = 0$. In this case, the film has a net TD density of $\Delta\rho = \rho_1 - \rho_i$. From Fig. 7(c) (dashed lines), the densities of dislocations 1 through 8 all begin to fall with increasing h, due to both annihilation and fusion reactions. The densities of dislocations 9 through 12 initially increases with increasing h due to the fusion reactions, then the densities of these dislocations also begins to fall. For larger values of h, ρ_2 through ρ_{12} monotonically decrease and asymptotically approach 0. However, ρ_1 asymptotically approaches a saturation value of $\Delta\rho$. The saturation behavior is most readily observed in Fig. 7(d) (dashed line), which shows on logarithmic axes the dependence of the ρ_T on h. ρ_T saturates to a value of $\Delta\rho$ because of the initial imbalance in TD density. From these results, it becomes obvious that in all cases in which the initial TD configuration has a net Burgers vector content, there will be saturation in the TD density regardless of the final film thickness. The origins of the net Burgers vector content in the film and the applicability of this concept will be developed shortly. First, however, we will show initial results of simulations of TD reduction.

Computer simulations provide a means to apply a simple set of physically motivated rules, in this case for interactions between TDs, and then consider the behavior of large ensembles of entities. The simulations were performed for the same slip geometry as described previously, namely, (001) growth of a cubic semiconductor with $a/2\langle 100\rangle\{111\}$ slip systems. In the simulation domain which was embedded in material with random boundary conditions (see below) the initial dislocation density ρ_0 was prescribed and normalized to r_A^{-2}. Since the growth trajectories of the dislocations is relevant for the simulations, each possible Burgers vector can lie on one of two $\{111\}$ planes. Thus, there are 24 possible specific Burgers vector/slip plane combinations. To facilitate the simulations, the line direction of the TDs was given as either $[\bar{1}\bar{1}2]$, $[1\bar{1}2]$, $[112]$, $[\underline{1}\bar{1}2]$ depending on whether the TD was on the (111), $(\bar{1}11)$, $(\bar{1}\bar{1}1)$, $(1\bar{1}1)$ plane, respectively. The initial dislocation type and position were randomly generated such that the type (1 through 24) and coordinate were independently generated. All pairs of TDs that fell within r_A of each other were considered in the context of possible reactions and those with favorable reactions were either removed (annihilation) or combined into one TD with a new Burgers vector (fusion). If there was no reaction, the pair was left undisturbed. Following the inquiry process, the film thickness increased by Δh and the TDs all translated laterally by $\Delta h \tan\psi$ in same sense as their line direction. The inquiry process was then repeated and all TDs within an annihilation radius of one another were either removed, combined, or left unchanged. This process of ''growth'' and inquiry was then repeated until the final film thickness was reached. If a TD exits the simulation domain, it was reintroduced randomly on the opposite edge of the domain from where it departed. In this manner there was no dislocation reduction through boundary disappearance. The random re-introduction also avoids artificial steady-state distribution profiles.

The simulations show remarkably close agreement with the results from the differential equations. In Figs. 7(a) and 7(c) we show on linear axes the thickness dependence of the density of the 12 different populations from the simulations (solid lines). The monotonically decreasing densities with increasing h correspond to the TDs generated from surface nucleation (inclined Burgers vectors). The TDs with initially increasing densities correspond to the TDs with Burgers vectors parallel to the film/substrate interface. For this comparison, the numerical solutions for the coupled differential equations were obtained for $r_A = r_F$ and $M = 1$. Note that the simulation results also lead to $1/h$ scaling behavior and saturation behavior.

We have demonstrated that net Burgers vector content in the TD density leads to saturation behavior. For a large area film, the net Burgers vector content in the total TD population should be nearly zero. However, for the geometrically enhanced TD reduction, the relevant area for TD annihilations and fusion reactions is $\sim h^2 \tan^2\psi \approx h^2$. This is also the relevant area to consider TD density fluctuations. The total TD density $\rho_T(\mathbf{r})$ may be written as a sum of the individual densities, i.e.,

$$\rho_T(\mathbf{r}) = \sum_i \rho_i(\mathbf{r}) = \overline{\rho} + \sum_i \Delta\rho_i(\mathbf{r}), \tag{12}$$

where $\rho_i(\mathbf{r})$ is the spatially dependent density of the ith type of TD, $\overline{\rho}$ is the average TD density (averaged over the area of the film), and $\Delta\rho_i(\mathbf{r})$ is the spatial fluctuation of the density of the ith type of TD. Since the sampling area for TD reactions is $\sim h^2$, the fluctuations in any particular density should only be considered for sampling areas greater than h^2. The saturation behavior may result from local net TD Burgers vector content. Thus the saturation density $\rho_s(r)$ will vary locally and can be approximated by a local total Burgers vector summation normalized by the magnitude of the Burgers vector, i.e.,

$$\rho_s(\mathbf{r}) \approx \frac{1}{b}\left|\sum_{i=1}^{N} \rho_i(\mathbf{r})\mathbf{b}_i\right|, \tag{13}$$

where $\mathbf{b}_i$ is the Burgers vector of the ith type of TD, b is the magnitude of $\mathbf{b}_i$, and N is the number of unique TD families. Note that this equation should properly describe fluctuations in the net TD Burgers vector content. Again, the sampling area for $\rho_s(r)$ should be on the order of h^2.

Presently, we can only speculate on the physical origin of the fluctuations in the net Burgers vector content of the TDs. It is possible that early in the TD generation process, the MD have long glide lengths since there are few other MDs that act as barriers to glide. If a limited number of sources are active in the initial generation process, the TDs on any individual half-loop may become separated by distances well in excess of h. If the TDs from a specific source are blocked by an obstacle, for instance an orthogonal MD[14]

or a cluster of MDs, then there can be local fluctuations in the Burgers vector content of the TDs. Unfortunately, the generation problem still remains poorly understood and further interpretation of the TD saturation requires further experiments.

VI. CONCLUSIONS

We have considered the general problem of the reduction of TD density in homogeneous buffer layers. The physical mechanisms responsible for TD reduction are reactions between TDs that lead to either annihilation or fusion. These reactions are only possible if the TDs have a minimum separation distance smaller than a physically prescribed interaction distance (annihilation radius or fusion radius). It has been established that in homogeneous buffer layers the distance between TDs is governed by geometrical factors such as the inclination of the TDs with respect to the free surface of the layer. As a result of layer growth, the point that a TD intersects the free surface will change. This is effectively equivalent to lateral motion of the TD and it leads to enhanced probability of annihilation if the TDs have a set of different trajectories.

We have specifically considered the crystallography of TDs and their reactions in fcc semiconductors. On the basis of this approach, the simple $1/h$ scaling law for TD reduction has been derived in the most general form and also for a series of coupled differential equations describing TD reduction in cubic semiconductors. The $1/h$ scaling behavior was also demonstrated in computer simulations of TD reduction. Additionally, we show that net Burgers vector content in the TDs must lead to saturation behavior. On this basis, we propose that saturation is a consequence of fluctuations in the net Burgers vector content in the film with a wavelength in excess of the characteristic sampling length.

ACKNOWLEDGMENTS

This work was supported in part by the UC MICRO program in conjunction with Hughes Aircraft corporation, by the AFOSR through Contract No. F49620-95-1-0394 (Dr. Gerald Witt contract monitor), by the NSF MRL program Grant No. DMR-9123048, and by the Max Planck Society. Additional support for GEB was provided by an Alexander-von-Humbolt Fellowship.

[1] L. B. Freund, Mater. Res. Bull. **17**, 52 (1992).
[2] J. Y. Tsao, *Materials Fundamentals of Molecular Beam Epitaxy* (Academic, New York, 1993).
[3] E. A. Fitzgerald, G. P. Watson, R. E. Proano, D. G. Ast, P. D. Kirchner, G. D. Petit, and J. M. Woodall, J. Appl. Phys. **65**, 2220 (1989).
[4] T. J. Gosling and J. R. Willis, J. Mech. Phys. Solids **42**, 1199 (1994).
[5] G. E. Beltz and L. B. Freund, Phys. Status Solidi B **180**, 303 (1993).
[6] P. Sheldon, K. M. Jones, M. M. Al-Jassim, and B. G. Yacobi, J. Appl. Phys. **63**, 5609 (1988).
[7] M. Tachikawa and M. Yamaguchi, Appl. Phys. Lett. **56**, 484 (1990).
[8] H. Okamoto, Y. Watanabe, Y. Kadota, and Y. Ohmachi, Jpn. J. Appl. Phys. **26**, L1950 (1987).
[9] N. Hayafuji, S. Ochi, M. Miyashita, M. Tsugami, T. Murotani, and A. Kawagishi, J. Cryst. Growth **93**, 494 (1988).
[10] N. Hayafuji, M. Miyashita, T. Mishimura, K. Kadoiwa, H. Kumabe, and T. Murotani, Jpn. J. Appl. Phys. **29**, 2371 (1990).
[11] J. P. Hirth and J. Lothe, *Theory of Dislocations*, 2nd ed. (Wiley, New York, 1982).
[12] A. A. Kusov and V. I. Vladimirov, Phys. Status Solidi B **138**, 135 (1986).
[13] M. Y. Martisov and A. E. Romanov, Sov. Phys. Solid State **32**, 1101 (1990).
[14] L. B. Freund, J. Appl. Phys. **68**, 2073 (1990).